NANO LETTERS

pubs.acs.org/NanoLett

Letter

Multiscale Photonic Emissivity Engineering for Relativistic Lightsail Thermal Regulation

John Brewer, Matthew F. Campbell, Pawan Kumar, Sachin Kulkarni, Deep Jariwala, Igor Bargatin, and Aaswath P. Raman*

Cite This: *Nano Lett.* 2022, 22, 594–601

Read Online

ACCESS | Metrics & More | Article Recommendations | Supporting Information

ABSTRACT: The Breakthrough Starshot Initiative aims to send a gram-scale probe to our nearest extrasolar neighbors using a laser-accelerated lightsail traveling at relativistic speeds. Thermal management is a key lightsail design objective because of the intense laser powers required but has generally been considered secondary to accelerative performance. Here, we demonstrate nanophotonic photonic crystal slab reflectors composed of 2H-phase molybdenum disulfide and crystalline silicon nitride, highlight the inverse relationship between the thermal band extinction coefficient and the lightsail's maximum temperature, and examine the trade-off between minimizing acceleration distance and setting realistic sail thermal limits, ultimately realizing a thermally endurable acceleration minimum distance of 23.3 Gm. We additionally demonstrate multiscale photonic structures featuring thermal-wavelength-scale Mie resonant geometries and characterize their broadband Mie resonance-driven emissivity enhancement and acceleration distance reduction. More broadly, our results highlight new possibilities for simultaneously controlling optical and thermal response over broad wavelength ranges in ultralight nanophotonic structures.

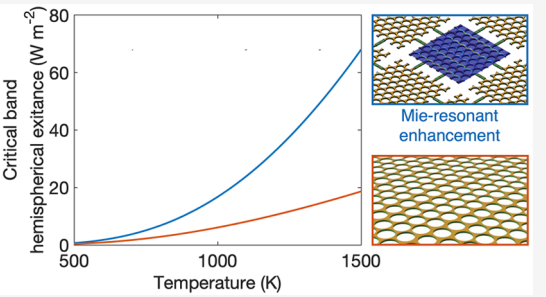

KEYWORDS: *Starshot, Lightsail, Photon Momentum, Infrared, Nanophotonics, Mie Resonance, Photonic Crystal Reflector, 2D Materials, Silicon Nitride, Molybdenum Disulfide*

Interstellar travel is a fundamental scientific and engineering challenge currently beyond the capability of advanced nuclear pulse[1] and fusion power-based[2−4] engines. An alternative approach proposed by the Breakthrough Starshot Initiative is to use a laser-propelled lightsail carrying a gram-scale probe at relativistic speeds to visit Earth's nearest candidate habitable exoplanet, Proxima Centauri B[5−7] within 20 years. Lightsails are ultralightweight, highly reflective surfaces propelled via photon momentum transfer[8] and are central to this remarkable potential capability. Lightsail-driven vehicles have been extensively studied for solar,[9−12] astrophysical,[13,14] and laser[15−18] sources. In the final case, relativistic lightsail design and material selection faces an extreme set of demands due to the target velocity requiring the use of gigawatt-scale light irradiances on the sail. The high laser irradiances in turn impose strong material, mechanical, and optical constraints for functional sail design.[19] Accelerative performance necessitates high broadband reflectivity to accelerate the sail and payload to its target velocity as quickly as possible, and to account for red-shifting due to the relativistic velocities involved. In addition, sail mass should be minimized, and sail shape[20] or patterning[21] should result in stable beam riding even when faced with nonideal beam shapes or alignments.[22] Sail survivability motivates the need for sufficient mechanical robustness to survive both extreme acceleration-induced forces and its interaction with the interstellar medium.[23−25] Finally, ensuring sail survivability requires vanishingly small absorptivities over the red-shifted laser band to prevent excessive heating, as well as sufficient emissivity to radiatively dissipate heat generated by any residual laser band absorptivity. Solutions to these criteria have only recently come within reach through advances in nanofabrication,[26−28] radiative cooling,[29,30] and nanophotonics.[31−34]

Pioneering work on relativistic lightsails[19] has included passive beam-riding stability[21,35,36] and maximizing reflectivity on a per-mass basis[37,38] in sails composed primarily of Si, SiO_2,[21,35,37,38] and Si_3N_4.[38,39] In these works, the sail's temperature has largely been a secondary consideration rather than a primary target to be minimized. Here, we propose a method to select sail designs by co-optimizing both their thermal performance and reflectivity, and explore for the first time the use of MoS_2 as a highly reflective material for

Received: August 23, 2021
Revised: January 3, 2022
Published: January 11, 2022

https://doi.org/10.1021/acs.nanolett.1c03273
Nano Lett. 2022, 22, 594−601

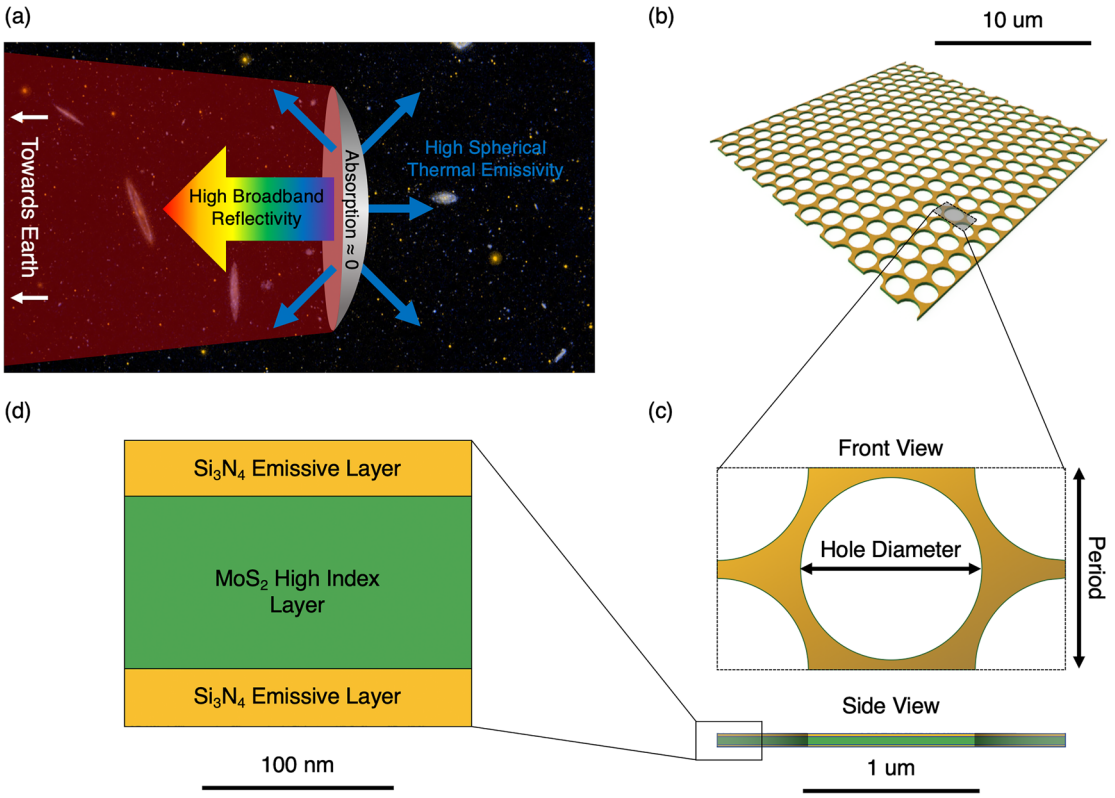

Figure 1. Photonic sail design. (a) Schematic diagram demonstrating relevant optical considerations for an accelerating lightsail. (b) Section of sail with hole diameter to period ratio of 90%. (c) Front and side view of single design period. (d) Enlarged view of multilayer structure. Yellow regions represent Si_3N_4 while green regions represent MoS_2.

photonic lightsails. Furthermore, we demonstrate a multiscale photonic structure that simultaneously optimizes for acceleration distance and enhances thermal emissivity to reduce sail temperatures.

Our lightsail design is based on a multilayer 2D photonic crystal slab-based geometry that features a molybdenum disulfide (MoS_2) reflective core layer surrounded on both sides by silicon nitride (Si_3N_4) emissive layers. Figure 1a illustrates the general optical considerations of lightsail design, while Figure 1b–d shows the geometric parameters we investigated in our periodic concept sails. While previous work has discussed the possible use of MoS_2 for laser-driven lightsails,[19] its use in photonic sail designs is still unexplored. Other materials such as diamond and silicon have been suggested but pose challenges due to high vacuum phase instability,[40] thermal[41] or stress[42] based band narrowing effects, or surface states,[43−45] all of which could cause absorption.

We chose to investigate designs employing MoS_2 for four key reasons. The first is its high refractive index in the Doppler-shifted laser band, ranging from n = 3.66−3.73, making it a desirable reflective material. Second, its high bandgap energy gives headroom for thermal bandgap narrowing effects that can increase the film's absorptivity.[46,47] Third, monolayer grown MoS_2 samples demonstrate zero absorption in the laser bandwidth within ellipsometric measurement limits.[48] Finally, large area monolayer samples have been fabricated successfully, a significant step toward future lightsail-scale films.[49−51] Si_3N_4 has also been recently investigated for lightsails[38,39,52] and remains a promising candidate due to its mature fabricability, low density, and high decomposition temperatures.[53,54] Recent work has demonstrated LPCVD-grown material absorption coefficients of order 10^{-4} cm^{-1}, a value currently limited by the presence of microvoids and hydrogen impurities.[55] Furthermore, Si_3N_4 has intrinsic emissivity characteristics in the 5−14 μm wavelength range[56] that match well with the sail's nominal operating temperature of 500−1000 K.

We employed a trilayer composite sandwich structure that provides high reflectivity in a lightweight and thermally robust package due to the core MoS_2 layer's superior ratio of refractive index to mass and the sail's large emissive area for cooling from the two Si_3N_4 face layers. In addition to the mass reduction benefits, our design provides reflective enhancement through coupling to broadband guided modes, building on conventional photonic crystal slab theory.[32] While we used this as the basis of our design, the extreme performance required of the lightsail necessitates departures from typical photonic crystal reflectors. Previous nanoscale photonic crystal reflectors in the literature have not been designed specifically for the severe mass constraints, large laser bandwidth, and optimized thermal emissivity that are required for the intended lightsail mission. Finally, our design is fully connected and requires no additional substrate to function as a standalone sail, offering an important structural advantage. However, a large corrugated support backbone may be necessary in practice to help the sail withstand extreme accelerative forces.[57] This structure would provide macroscale sail curvature to increase stability and mechanical robustness[20] while additionally limiting crack propagation in our proposed designs due to patterned hole-induced stress concentrations.

To benchmark sail designs, we assumed typical design parameters for Breakthrough Starshot: a uniform I = 10 $\frac{GW}{m^2}$

https://doi.org/10.1021/acs.nanolett.1c03273
Nano Lett. 2022, 22, 594−601

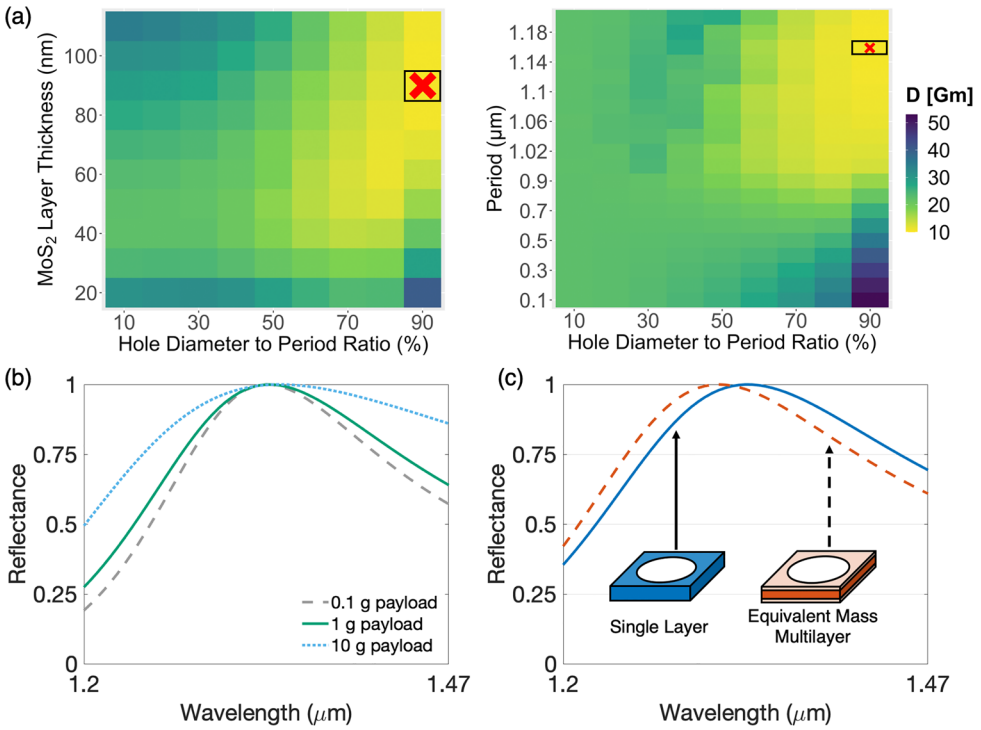

Figure 2. Reflective properties of multilayer photonic sail structures. (a) Color maps of minimum acceleration distance designs for a 1 g payload as a function of the most sensitive geometric parameters. Each color map represents a two parameter slice of the five parameter design space composed of the period/lattice constant, the hole diameter-to-period ratio, and the thicknesses of each of the three layers. Tile colormap shows the acceleration distance for the design specified by the parameter values on the axis, shown for top and bottom Si_3N_4 layer thicknesses of 5 nm, the optimal values to minimize acceleration distance. Outlined tiles marked with the red " × " show the parameter values of the lowest acceleration distance design in our simulation space. (b) Dependence of lowest acceleration distance sail reflection spectra on payload mass over the Doppler-shifted laser wavelength range. The optimal sails corresponding to payload masses of 0.1, 1, or 10 g have unladen masses of 1.17, 1.3, or 2.27 g respectively. Thus, as the given payload mass decreases, sail mass reduction is a greater factor in decreasing acceleration distance than reflectivity spectra enhancement. (c) Demonstration of spectral reflectance perturbation due to the addition of lower index, high emissivity Si_3N_4 layers. The red-shifted reflectance spectra resulting from the multilayer design results in an increased acceleration distance in order to enable necessary thermal benefits. Insets provide schematic diagrams of sail designs corresponding to plot colors.

laser irradiance on the sail, a laser output wavelength of $\lambda = 1.2$ μm, a 10 m^2 sail area, and a 1 g chip payload mass unless otherwise stated. The acceleration distance figure of merit, as defined by Jin et al.[38] is

$$D = \frac{c^3}{2I}(\rho_{\text{payload}} + \rho_{\text{sail}}) \int_0^{0.2} \frac{h(\beta)}{R(\lambda(\beta))}\, d\beta \quad (1)$$

where $h(\beta) = \frac{\beta}{(1-\beta)^2\sqrt{1-\beta^2}}$, I is the laser irradiance in $\frac{W}{m^2}$, ρ is areal density in $\frac{kg}{m^2}$, β is the unitless relative velocity (the ratio of the sail velocity to the speed of light), and $R(\lambda(\beta))$ is the spectral reflectance over the Doppler-shifted laser band. It is worth noting that a constant irradiance term with respect to β implies the use of laser power throttling to ensure the incident power on the sail remains constant throughout its acceleration. A detailed explanation of this can be found in the Supporting Information of Campbell et al.[20]

Optimizing the period and hole diameter of the patterned holes allows for high transmission and reflection bands of varying spectral bandwidth.[32] Figure 2a,b demonstrates the dependence of acceleration distance on key design parameters in our sail design space. Our optimal acceleration distance merited design has a period of 1.16 μm, a hole period to diameter ratio of 90%, 5 nm thick emissive Si_3N_4 layers, and a 90 nm thick MoS_2 reflective core, placing it in a regime of very low thickness values relative to the lattice constant, <0.1a. Thinning of the high-index core maintains access to broadband Fabry−Perot-like reflection modes at normal incidence with the added effect of minimizing the overall sail mass. This demonstrates the broad range of possible acceleration distance values that our design space encompasses.

The precise payload chip mass, though likely to be roughly 1 g, has not yet been determined for the actual craft, such that understanding the effect of mass on our optimal design is critical. Note that payload mass can be converted to the areal density value shown in eq 1 according to $\rho_{\text{payload}} = m_{\text{payload}}/A_{\text{sail}}$. Figure 2b plots the laser band reflection spectra of the lowest acceleration distance design for three payload masses, demonstrating that as the payload mass decreases, reducing the sail's mass is rewarded more than improving its reflectance spectrum. This means that sail mass becomes a stronger consideration when the payload mass is small. A further analysis showing the minimum acceleration distance versus payload mass can be found in the Supporting Information, which is corroborated by results in Jin et al.[38]

The Si_3N_4 layers we have introduced are necessary to enhance thermal emissivity; however, these can also have the effect of shifting the peak of the sail reflection spectra to lower wavelengths compared to single-layer MoS_2-only designs, as shown in Figure 2c. The shift results in a ∼6% increase in the acceleration distance figure of merit due to the monotonically

https://doi.org/10.1021/acs.nanolett.1c03273
Nano Lett. 2022, 22, 594−601

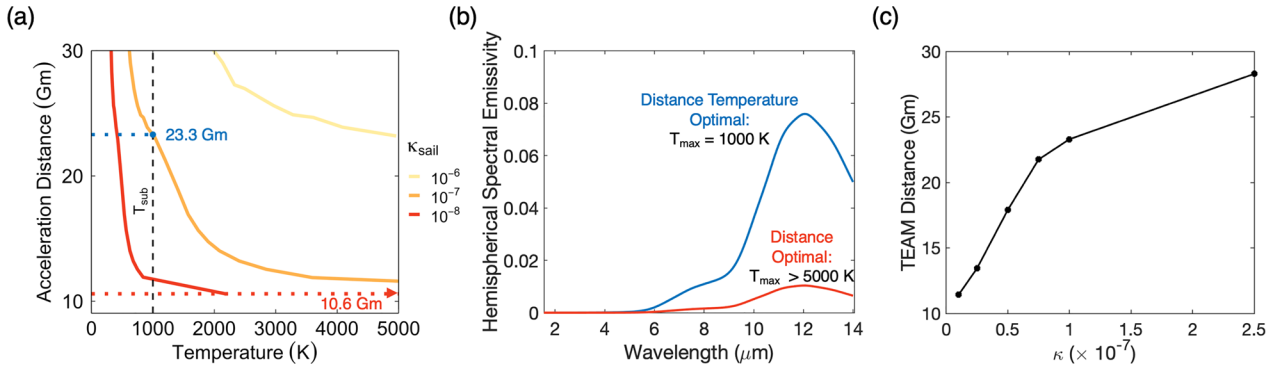

Figure 3. Emissive properties of multilayer photonic sail structures for a 1 g payload. (a) Minimum acceleration distance as a function of temperature for three imposed values of sail material extinction coefficient. The vertical black dotted line marks the defined ultrahigh vacuum thermal limit. On the central curve ($\kappa = 10^{-7}$) the blue point and accompanying line mark the acceleration distance and temperature of the TEAM design. The TEAM design is that which obtains the TEAM distance, that is, that which has the shortest acceleration distance among those design alternatives whose temperatures do not exceed the thermal limit. The red dotted line marks the minimum acceleration distance achievable in our design space and demonstrates that the corresponding design has a peak temperature >5000 K for $\kappa = 10^{-7}$, meaning the theoretical corresponding red point (marking the intersection of the orange curve with the red dotted line) is not visible. The solid red curve corresponds to a simulated value of $\kappa = 10^{-8}$, which shows a solution below 5000 K, but it is still more than double the enforced thermal limit. Decreasing κ has the effect of decreasing the TEAM distance from 23.3 to 11.4 Gm. (b) Comparison of the hemispherical emissivity spectra, that is, the direction-averaged spectral emissivity, of the simple acceleration merited design corresponding to the theoretical off plot red point in (a) versus acceleration distance-temperature comerited design corresponding to the blue point in (a). Calculated maximum temperatures of the designs are also provided. (c) Plot showing thermally endurable acceleration minimum (TEAM) distance for six selected values of κ, connected to show trended behavior. Values of κ greater than the plot domain have no solution within our simulated sail set, meaning layers of Si_3N_4 thicker than 110 nm are necessary to maintain thermal integrity of the sail in flight.

increasing nature of $h(\beta)$ in eq 1. This highlights that having high reflectivity at longer Doppler-shifted laser band wavelengths is more beneficial then at shorter wavelengths given a constant irradiance on the sail. We note that since the designs shown in Figure 2c have identical masses of ∼1.3 g, this effect is attributable to the change in the refractive index profile alone.

Our simulated sail design set resulted in an optimal reflective design with an acceleration distance of 10.6 Gm when carrying a 1 g payload, comparable in performance to current leading designs.[38] Importantly, our methodology takes into account all mass required for acceleration and cooling and our design does not require a connecting support structure. If necessary, adding a 1 g mechanical backbone would provide additional structural stability and increase the acceleration distance to 15.2 Gm. Furthermore, the geometry of this design is not computationally optimized, and optimization could yield still lower acceleration distances. While the current design is competitive with the best shown previously,[38] we will show that adding realistic thermal considerations increases acceleration distances by 120%.

Lightsails can easily disintegrate during acceleration, making sail integrity just as critical as reflection-driven performance metrics. While the sail must exhibit extremely low absorptivity, this value is finite in practice and the sail's temperature will increase due to the high incident laser irradiance. Interaction with the interstellar medium at relativistic speeds could also cause heating.[23] Additionally, the sail's component materials can become more absorptive as their temperature rises, raising concerns about thermal runaway[58] and increasing the probability of sail thermal failure. Our approach seeks to optimize sail design in terms of its acceleration characteristics while ensuring sufficient radiative cooling characteristics to maintain sail integrity. We adopt the ultrahigh vacuum (UHV) sublimation temperature $T_{\text{sublimation}}$ of the sail materials as a thermal limit. Note that since the UHV sublimation temperature is less than the 1 atm melting temperature selected as the thermal limit in other recent lightsail studies,[21,35] this represents a conservative design decision. In our case, we adopted $T_{\text{limit}} = T_{\text{sublimation,MoS}_2} \sim 1000$ K, which is the lower UHV sublimation point among the two materials used[59,60] (see Supporting Information).

To our knowledge, the temperature-dependent absorption properties of MoS_2 have only been investigated in the Doppler-shifted laser band up to 500 K using ellipsometric methods.[61] This initial data suggests that the absorptivity of MoS_2 as a function of temperature may actually decrease while its refractive index stays relatively constant, even in the presence of thermally activated band narrowing. Investigation at higher temperatures with higher sensitivity will be necessary to fully determine thermal runaway-based effects. We further note that ellipsometric methods, which were used to generate the optical constant data in our simulations, cannot reliably measure absorptivities of less than 1% of the incoming source intensity. This strongly highlights the need for sensitive measurements of materials used for relativistic lightsails using techniques such as photothermal deflection[62] and photocurrent[63] spectroscopy. New growth methods such as chemical vapor transport and self-flux growth[64−66] offer the possibility of producing electronically thick bulk film samples having optical quality comparable to or better than the lowest values reported in the optical constant data set used for simulation and analysis in this work.[48]

We implicitly calculated the maximum temperature T_{max} reached by each sail in our space of over 3×10^5 designs using the following equation

$$P_{\text{sail}}\alpha_{\text{sail}} = 2A_{\text{sail}}\int_a^b \frac{c_1}{\lambda^5}\cdot\frac{\epsilon_{\text{sail}}(\lambda)}{e^{c_2/\lambda T_{\text{max}}} - 1}\,\mathrm{d}\lambda \tag{2}$$

where P_{sail} is the incident laser power on the sail, α is the laser band spectrally averaged integrated absorptivity of the sail, A_{sail}

https://doi.org/10.1021/acs.nanolett.1c03273
Nano Lett. 2022, 22, 594−601

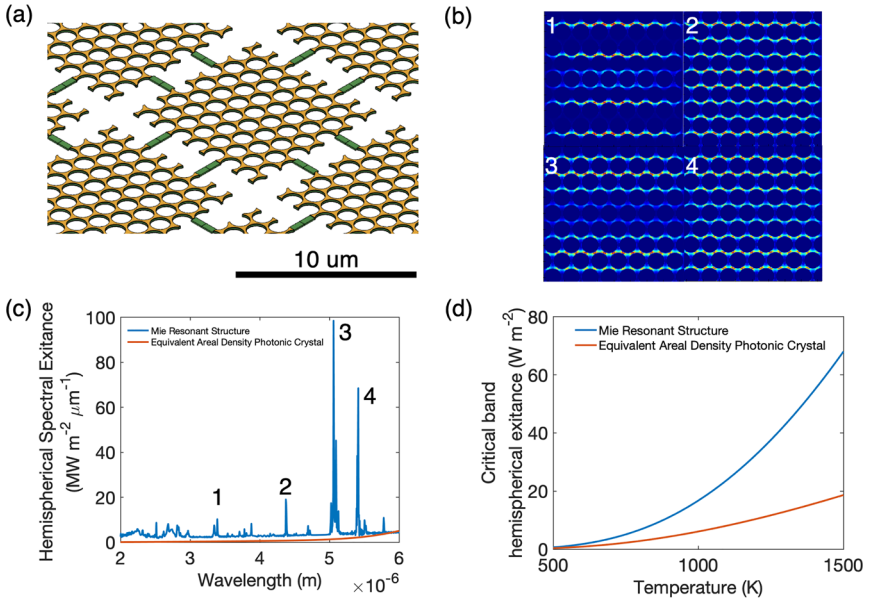

Figure 4. (a) Mie resonant enhancement schematic diagram illustrating the proposed multiscale Mie resonator design. The green strips show the possibility of scaffolds used to support the Mie resonator structure. (b) Spatial absorption profiles of Mie resonances in (c) corresponding to the respectively labeled spectral peaks. (c) Hemispherical exitance of Mie resonant structure versus conventional photonic crystal structure, calculated at a temperature of 1000 K, demonstrating a pathway for possible emissivity enhancement. (d) Demonstration of spectrally integrated hemispherical exitance enhancement as a function of temperature.

is the area of a single side of the sail, the factor of 2 accounts for the emission by Si_3N_4 on both sides of the sail, a = 1.55 μm, b = 14.05 μm, $c_1 = 2\pi hc^2$, $c_2 = hc/k_b$, h is Planck's constant, c is the speed of light, k_b is Boltzmann's constant, and ϵ_{sail} is the spectral sail emissivity (see Supporting Information).

Our initial designs leveraging conventional photonic crystal theory have desirable properties from an acceleration merit standpoint, but their thermal band radiant exitance is highly dependent on the intrinsic spectral emissivity of their component materials. In the case of lightsails, a trade-off exists between thermoregulation and acceleration distance. In general, for a given sail diameter, increasing mass increases acceleration distance, while increasing emissive material mass enhances heat dissipation. However, greater material mass can also result in greater laser absorption. We applied these considerations by simulating our sail designs at three material extinction coefficient values of $\kappa = 10^{-8}$, 10^{-7}, and 10^{-6} for both Si_3N_4 and MoS_2 over the laser band. These coarse choices are due to the aforementioned lack of material extinction coefficient data in the Doppler-shifted laser band. We then used the resulting absorptivity values to show the relationship between acceleration distance and operating temperature for a given κ in Figure 3a. These results can also be stated in terms of assumed total sail absorptivity (Supporting Information). This result clearly illustrates the effect of extinction coefficient on sail survivability. As extinction coefficient values are increased for the constituent materials, acceleration distances below a threshold value become thermally impossible to achieve. The horizontal lines are iso-acceleration distance lines, and their intersections with the curves mark extinction coefficients for which sails with a given acceleration distance value exist.

We now define a new and final composite figure of merit for our sail design space, which we call the thermally endurable acceleration minimum (TEAM) distance value. The TEAM distance value for a design space is the minimum acceleration distance among designs where $T_{sail,max} < T_{limit}$. Likewise, the TEAM sail design is the sail configuration that results in the TEAM distance value. Minimizing the TEAM distance is desirable, but we emphasize that this is not a sail metric per se; rather, it is a summary value that can be easily reported to compare design approaches and sail data sets, rather than individual sails. Given laser parameters, payload mass, and sail architectures with known acceleration distances, TEAM distance depends on three quantities: the previously set maximum allowable sail temperature determined by the UHV sublimation limit (and therefore the high vacuum properties of the materials system used for sail design), the laser band absorption properties of the sail, and the thermal emissivity of the sail. After both high vacuum thermodynamic and high sensitivity absorption properties of candidate materials are fully determined, this can act as a simple way to compare design spaces without ambiguity.

Using our analysis framework for an imposed extinction coefficient of $\kappa = 10^{-7}$, we demonstrate a TEAM distance value of 23.3 Gm, a 12.7 Gm accelerative penalty relative to the original 10.6 Gm minimum distance, which prevents MoS_2 sublimation by limiting the sail's peak temperature to T_{max} = 1000 K. Addition of a 1 g mechanical backbone results in a larger TEAM value of 76.7 Gm. This design has a period of 1.08 μm, a hole diameter to period ratio of 0.1, a top Si_3N_4 emissive layer of 10 nm, a 50 nm thick high index MoS_2 layer, and a 5 nm bottom Si_3N_4 layer. Our TEAM-derived sail design has a smaller hole radius and thicker Si_3N_4 layers relative to the original 10.6 Gm design. Comparing the spectral hemispherical emissivity values of the two designs (Figure 3b) reveals that the thicker, larger emissive area design is necessary to radiate away excess energy and survive. The TEAM design has an approximately 8× higher peak emissivity value due to the presence of more Si_3N_4 in the photonic crystal structure. Figure 3c shows TEAM value as a function of κ in the laser band. When κ increases, the TEAM distance increases, placing

https://doi.org/10.1021/acs.nanolett.1c03273
Nano Lett. 2022, 22, 594−601

firm bounds on allowable material absorption given a target acceleration distance.

Previously developed photonic lightsail designs are limited to single-scale photonic features and their associated thermal characteristics. However, a multiscale segmented design architecture could yield additional thermal benefits without incurring a mass penalty. To explore this, we proposed and investigated an emissivity-enhancing multiscale Mie resonant structure with thermal wavelength-scale Mie resonators patterned with laser-wavelength-scale photonic crystal features (Figure 4a). These multiscale photonic structures yield a large number of resonant peaks over desired peak thermal wavelengths that collectively enhance the total hemispherical emittance of the sail. This is reminiscient of nanophotonic light trapping approaches to solar absorption, where numerous peaks contribute to absorption enhancment.[67,68] Our design is composed of two 30 nm emissive Si_3N_4 layers surrounding a 90 nm MoS_2 core. The patterned photonic crystal has a period of 1.14 μm with a 90% hole diameter to period ratio. The multiscale Mie structure is 8.55 μm by 8.55 μm with an overall period of 10 μm. The Mie structure achieved a temperature-constrained acceleration distance of 16.7 Gm compared to 24 Gm for a continuous non-Mie design with similar areal density. Importantly, the Mie structure's additional emissivity in the critical 2−6 μm band lowers the sail's peak temperature. Remarkably, the Mie resonant design has a 7.4 Gm shorter acceleration distance or a 43% decrease as compared to the equivalent continuous design. Because the areal density of Si_3N_4 between the compared designs is nearly the same, longer wavelength thermally emissive features will be maintained between the two designs, meaning the additional emissivity features in the critical band from 2 to 6 μm are key to enabling lower overall temperatures. The structure can be connected by a series of thin scaffolds while maintaining the presence of resonant modes. If further mechanical robustness is desired, a mechanical backbone could be added.

The spatial profiles of four resonant modes supported by the multiscale Mie-resonant structure are shown in Figure 4b, corresponding to four modes in the 2−6 μm band shown in Figure 4c. Figure 4c shows the hemispherical direction-averaged spectral exitance in this band, determined by weighting the hemispherically direction averaged emissivity spectrum of the device with the spectrum of a 1000 K blackbody. This wavelength band is critical for sail heat management due to the blackbody peak position at temperatures from 500−1000 K, as determined by Wien's law. Increases to sail emissivity in the 2−6 μm band will more strongly reduce overall sail temperatures in comparison to emissivity increases at longer wavelengths. The enhancement of in-band hemispherical exitance at a given temperature is demonstrated in Figure 4d, showing that at the previously suggested thermal limit of 1000 K, the islanded design has over 2.75× greater hemispherical exitance, with as much as 3.6× the hemispherical exitance at 1500 K. This showcases the utility of the multiscale Mie-resonant structures for thermal regulation of ultralight photonic structures.

In conclusion, we have demonstrated holistically viable multilayer 2D photonic reflector designs for laser-driven lightsails that are able to accelerate to one-fifth the speed of light over distances comparable to, and in some cases even exceeding, designs reported previously. We emphasize that our designs represent the entire sail structure and do not require additional backing material for emissivity enhancement, allowing for accurate modeling of payload-driven performance. To analyze such relativistic lightsail designs, we further proposed an analysis framework that accounts for both acceleration distance and peak temperature. We then proposed the thermally endurable acceleration minimum (TEAM) distance value as a summary statistic to determine the fastest-accelerating thermally stable sail design of a design set. This value is easily reportable and will allow researchers to compare their design sets, represented by a variety of materials and nanoscale geometries. Finally, we introduced a multiscale sail design employing thermal-wavelength-scale Mie-resonant features to enhance the mid-infrared emissivity of lightsails while preserving their underlying acceleration distance characteristics. Although relativistic lightsails impose stringent constraints, our multiscale photonic designs highlight intriguing optical capabilities that ultralight, nearly massless photonic structures can enable over an ultrabroadband wavelength range. This in turn heralds the possibility of new classes of ultralight photonic structures that can perform as well as conventional photonic structures for mass-constrained aerospace, imaging, and information processing applications.

■ ASSOCIATED CONTENT

Supporting Information

The Supporting Information is available free of charge at https://pubs.acs.org/doi/10.1021/acs.nanolett.1c03273.

Addtional information on methods, material optical constant data sets, figures of merit, payload mass considerations, and alternative Mie-resonance based design architectures (PDF)

■ AUTHOR INFORMATION

Corresponding Author

Aaswath P. Raman − *Department of Materials Science and Engineering, University of California, Los Angeles, Los Angeles, California 90095, United States*; Email: aaswath@ucla.edu

Authors

John Brewer − *Department of Materials Science and Engineering, University of California, Los Angeles, Los Angeles, California 90095, United States*; orcid.org/0000-0003-1878-8863

Matthew F. Campbell − *Department of Mechanical Engineering and Applied Mechanics, University of Pennsylvania, Philadelphia, Pennsylvania 19104, United States*; orcid.org/0000-0002-7611-0332

Pawan Kumar − *Department of Electrical and Systems Engineering, University of Pennsylvania, Philadelphia, Pennsylvania 19104, United States*; orcid.org/0000-0002-5764-2915

Sachin Kulkarni − *Department of Materials Science and Engineering, University of California, Los Angeles, Los Angeles, California 90095, United States*

Deep Jariwala − *Department of Electrical and Systems Engineering, University of Pennsylvania, Philadelphia, Pennsylvania 19104, United States*; orcid.org/0000-0002-3570-8768

Igor Bargatin − *Department of Mechanical Engineering and Applied Mechanics, University of Pennsylvania, Philadelphia, Pennsylvania 19104, United States*; orcid.org/0000-0003-0305-9932

https://doi.org/10.1021/acs.nanolett.1c03273
Nano Lett. 2022, 22, 594−601

Complete contact information is available at:
https://pubs.acs.org/10.1021/acs.nanolett.1c03273

Notes

The authors declare no competing financial interest.

■ ACKNOWLEDGMENTS

This work was supported by the Breakthrough Initiatives, a division of the Breakthrough Prize Foundation. J.B. is supported by a National Science Foundation Graduate Research Fellowship under Grants DGE-1650605 and DGE-2034835. It was also funded in part by a National Science Foundation CAREER award under Grant CBET-1845933.

■ REFERENCES

(1) Martin, A. R.; Bond, A. H. J. Nuclear pulse propulsion: a historical review of an advanced propulsion concept. *Journal of the British Interplanetary Society* **1979**, *32*, 283.
(2) Beals, K. A.; Beaulieu, M.; Dembia, F. J.; Kerstiens, J.; Kramer, D. L.; West, J. R.; Zito, J. A. *Project longshot: An unmanned probe to Alpha Centauri*; United States Naval Academy, 1988.
(3) Bond, A.; Group, P. D. S. *Project Daedalus: The final report on the BIS starship study*; British Interplanetary Society: London, England, 1978.
(4) Long, K.; Obousy, R.; Hein, A. Project Icarus: Optimisation of nuclear fusion propulsion for interstellar missions. *Acta Astronautica* **2011**, *68*, 1820−1829.
(5) Wagner, K.; Boehle, A.; Pathak, P.; Kasper, M.; Arsenault, R.; Jakob, G.; Kaufl, U.; Leveratto, S.; Maire, A.-L.; Pantin, E.; Siebenmorgen, R.; Zins, G.; Absil, O.; Ageorges, N.; Apai, D.; Carlotti, A.; Choquet, E.; Delacroix, C.; Dohlen, K.; Duhoux, P.; Forsberg, P.; Fuenteseca, E.; Gutruf, S.; Guyon, O.; Huby, E.; Kampf, D.; Karlsson, M.; Kervella, P.; Kirchbauer, J.-P.; Klupar, P.; Kolb, J.; Mawet, D.; N'Diaye, M.; de Xivry, G. O.; Quanz, S. P.; Reutlinger, A.; Ruane, G.; Riquelme, M.; Soenke, C.; Sterzik, M.; Vigan, A.; de Zeeuw, T. Imaging low-mass planets within the habitable zone of α Centauri. *Nat. Commun.* **2021**, *12*, 1−7.
(6) Dumusque, X.; Pepe, F.; Lovis, C.; Ségransan, D.; Sahlmann, J.; Benz, W.; Bouchy, F.; Mayor, M.; Queloz, D.; Santos, N.; Udry, S. An Earth-mass planet orbiting α Centauri B. *Nature* **2012**, *491*, 207−211.
(7) Parkin, K. L. The Breakthrough Starshot system model. *Acta Astronautica* **2018**, *152*, 370−384.
(8) Novotny, L.; Hecht, B. *Principles of Nano-Optics*, 2nd ed.; Cambridge University Press, 2012; p 448−473.
(9) Garwin, R. L. *Solar sailing-A practical method of propulsion within the solar system*; American Rocket Society, Inc., 1958.
(10) Drexler, K. E. *High performance solar sails and related reflecting devices*; Princeton University and American Institute of Aeronautics and Astronautics, 4th Conference on Space Manufacturing Facilities; Princeton University, Princeton, NJ, 1979.
(11) Davoyan, A. R.; Munday, J. N.; Tabiryan, N.; Swartzlander, G. A.; Johnson, L. Photonic materials for interstellar solar sailing. *Optica* **2021**, *8*, 722.
(12) Tsuda, Y.; Mori, O.; Funase, R.; Sawada, H.; Yamamoto, T.; Saiki, T.; Endo, T.; Kawaguchi, J. Flight status of IKAROS deep space solar sail demonstrator. *Acta Astronautica* **2011**, *69*, 833−840.
(13) Lingam, M.; Loeb, A. Propulsion of spacecraft to relativistic speeds using natural astrophysical sources. *Astrophysical Journal* **2020**, *894*, 36.
(14) Wentzel-Long, M.; Landis, G. A. Power Generation from Interplanetary and Interstellar Plasma and Magnetic Fields. *AIAA Propulsion and Energy 2020 Forum*, August 2020; AIAA: https://arc.aiaa.org/doi/10.2514/6.2020-3537, accessed May 25, 2021.
(15) Forward, R. L. Roundtrip interstellar travel using laser-pushed lightsails. *Journal of Spacecraft and Rockets* **1984**, *21*, 187−195.
(16) Kulkarni, N.; Lubin, P.; Zhang, Q. Relativistic spacecraft propelled by directed energy. *Astronomical Journal* **2018**, *155*, 155.
(17) Redding, J. L. Interstellar vehicle propelled by terrestrial laser beam. *Nature* **1967**, *213*, 588−589.
(18) Kipping, D. Relativistic light sails. *Astronomical Journal* **2017**, *153*, 277.
(19) Atwater, H. A.; Davoyan, A. R.; Ilic, O.; Jariwala, D.; Sherrott, M. C.; Went, C. M.; Whitney, W. S.; Wong, J. Materials challenges for the Starshot lightsail. *Nat. Mater.* **2018**, *17*, 861−867.
(20) Campbell, M. F.; Brewer, J.; Jariwala, D.; Raman, A. P.; Bargatin, I. Relativistic light sails need to billow. *Nano Letters* **2021**, DOI: 10.1021/acs.nanolett.1c03272.
(21) Salary, M. M.; Mosallaei, H. Photonic metasurfaces as relativistic light sails for doppler-broadened stable beam-riding and radiative cooling. *Laser and Photonics Reviews* **2020**, *14*, 1900311.
(22) Manchester, Z.; Loeb, A. Stability of a Light Sail Riding on a Laser Beam. *Astrophysical Journal* **2017**, *837*, L20.
(23) Hoang, T.; Lazarian, A.; Burkhart, B.; Loeb, A. The interaction of relativistic spacecrafts with the interstellar medium. *Astrophysical Journal* **2017**, *837*, 5.
(24) Hoang, T.; Loeb, A. Electromagnetic forces on a relativistic spacecraft in the interstellar medium. *Astrophysical Journal* **2017**, *848*, 31.
(25) Early, J. T.; London, R. A. Dust grain damage to interstellar laser-pushed lightsail. *Journal of Spacecraft and Rockets* **2000**, *37*, 526−531.
(26) Chou, S. Y.; Krauss, P. R.; Renstrom, P. J.; Chou, S. Y.; Krauss, P. R.; Renstrom, P. J. Imprint lithography with 25-nanometer resolution. *Science* **1996**, *272*, 85−87.
(27) Chen, Y. Nanofabrication by electron beam lithography and its applications: A review. *Microelectron. Eng.* **2015**, *135*, 57−72.
(28) Johnson, R. W.; Hultqvist, A.; Bent, S. F. A brief review of atomic layer deposition: From fundamentals to applications. *Mater. Today* **2014**, *17*, 236−246.
(29) Raman, A. P.; Anoma, M. A.; Zhu, L.; Rephaeli, E.; Fan, S. Passive radiative cooling below ambient air temperature under direct sunlight. *Nature* **2014**, *515*, 540.
(30) Rephaeli, E.; Raman, A.; Fan, S. Ultrabroadband photonic structures to achieve high-performance daytime radiative cooling. *Nano Lett.* **2013**, *13*, 1457−1461.
(31) Johnson, S. G.; Fan, S.; Villeneuve, P. R.; Joannopoulos, J. D.; Kolodziejski, L. A. Guided modes in photonic crystal slabs. *Physical Review B - Condensed Matter and Materials Physics* **1999**, *60*, 5751−5758.
(32) Fan, S.; Joannopoulos, J. D. Analysis of guided resonances in photonic crystal slabs. *Physical Review B - Condensed Matter and Materials Physics* **2002**, *65*, 1−8.
(33) Molesky, S.; Lin, Z.; Piggott, A. Y.; Jin, W.; Vucković, J.; Rodriguez, A. W. Inverse design in nanophotonics. *Nat. Photonics* **2018**, *12*, 659−670.
(34) Yu, N.; Capasso, F. Flat optics with designer metasurfaces. *Nat. Mater.* **2014**, *13*, 139−150.
(35) Salary, M. M.; Mosallaei, H. Inverse design of diffractive relativistic meta-sails via multi-objective optimization. *Advanced Theory and Simulations* **2021**, *4*, 2100047.
(36) Ilic, O.; Atwater, H. A. Self-stabilizing photonic levitation and propulsion of nanostructured macroscopic objects. *Nat. Photonics* **2019**, *13*, 289−295.
(37) Ilic, O.; Went, C. M.; Atwater, H. A. Nanophotonic heterostructures for efficient propulsion and radiative cooling of relativistic light sails. *Nano Lett.* **2018**, *18*, 5583−5589.
(38) Jin, W.; Li, W.; Orenstein, M.; Fan, S. Inverse design of lightweight broadband reflector for relativistic lightsail propulsion. *ACS Photonics* **2020**, *7*, 2350−2355.
(39) Gao, R.; Kim, Y.; Kim, L.; Kelzenberg, M. D.; Ilic, O.; Atwater, H. A. Self-stabilizing silicon nitride lightsails. *Conference Proceedings - Lasers and Electro-Optics Society Annual Meeting-LEOS 2020*; 2020 May 4−5, virtual conference; https://www.osapublishing.org/abstract.cfm?uri=CLEO_SI-2020-SF3J.6

(40) Zazula, J. M. *On graphite transformations at high temperature and pressure induced by absorption of the LHC beam*; CERN: Geneva, Switzerland, 1997; p 15.
(41) Nguyen, H. T.; Rougieux, F. E.; Mitchell, B.; Macdonald, D. Temperature dependence of the band-band absorption coefficient in crystalline silicon from photoluminescence. *J. Appl. Phys.* **2014**, *115*, 043710.
(42) Kang, T. K. Evidence for silicon bandgap narrowing in uniaxially strained MOSFETs subjected to tensile and compressive stress. *IEEE Electron Device Lett.* **2012**, *33*, 770−772.
(43) Jackson, W. B.; Johnson, N. M.; Biegelsen, D. K. Density of gap states of silicon grain boundaries determined by optical absorption. *Appl. Phys. Lett.* **1983**, *43*, 195−197.
(44) Baehr-Jones, T.; Hochberg, M.; Scherer, A. Photodetection in silicon beyond the band edge with surface states. *Opt. Express* **2008**, *16*, 1659.
(45) Cloutier, S. G.; Kossyrev, P. A.; Xu, J. Optical gain and stimulated emission in periodic nanopatterned crystalline silicon. *Nat. Mater.* **2005**, *4*, 887−891.
(46) Mak, K. F.; Lee, C.; Hone, J.; Shan, J.; Heinz, T. F. Atomically thin MoS_2: A new direct-gap semiconductor. *Phys. Rev. Lett.* **2010**, *105*, 2−5.
(47) Böker, T.; Severin, R.; Müller, A.; Janowitz, C.; Manzke, R.; Voß, D.; Krüger, P.; Mazur, A.; Pollmann, J. Band structure of MoS_2, $MoSe_2$ and a-$MoTe_2$: Angle-resolved photoelectron spectroscopy and ab initio calculations. *Physical Review B - Condensed Matter and Materials Physics* **2001**, *64*, 1−11.
(48) Ermolaev, G. A.; Stebunov, Y. V.; Vyshnevyy, A. A.; Tatarkin, D. E.; Yakubovsky, D. I.; Novikov, S. M.; Baranov, D. G.; Shegai, T.; Nikitin, A. Y.; Arsenin, A. V.; Volkov, V. S. Broadband optical properties of monolayer and bulk MoS_2. *npj 2D Materials and Applications* **2020**, *4*, 1−6.
(49) Dumcenco, D.; Ovchinnikov, D.; Marinov, K.; Lazić, P.; Gibertini, M.; Marzari, N.; Sanchez, O. L.; Kung, Y.-C.; Krasnozhon, D.; Chen, M.-W.; Bertolazzi, S.; Gillet, P.; Fontcuberta i Morral, A.; Radenovic, A.; Kis, A. Large-area epitaxial monolayer MoS_2. *ACS Nano* **2015**, *9*, 4611−4620.
(50) Li, M.; Yao, J.; Wu, X.; Zhang, S.; Xing, B.; Niu, X.; Yan, X.; Yu, Y.; Liu, Y.; Wang, Y. P-type doping in large-area monolayer MoS_2 by chemical vapor deposition. *ACS Appl. Mater. Interfaces* **2020**, *12*, 6276−6282.
(51) Nie, C.; Yu, L.; Wei, X.; Shen, J.; Lu, W.; Chen, W.; Feng, S.; Shi, H. Ultrafast growth of large-area monolayer MoS_2 film via gold foil assistant CVD for a highly sensitive photodetector. *Nanotechnology* **2017**, *28*, 275203.
(52) Myilswamy, K. V.; Krishnan, A.; Povinelli, M. L. Photonic crystal lightsail with nonlinear reflectivity for increased stability. *Opt. Express* **2020**, *28*, 8223.
(53) Nishi, Y.; Doering, R. *Handbook of semiconductor manufacturing technology*; CRC Press, 2000.
(54) Haynes, W. M. *CRC handbook of chemistry and physics*; CRC Press, 2014.
(55) Ji, X.; Roberts, S.; Corato-Zanarella, M.; Lipson, M. Methods to achieve ultra-high quality factor silicon nitride resonators. *APL Photonics* **2021**, *6*, 071101.
(56) Kischkat, J.; Peters, S.; Gruska, B.; Semtsiv, M.; Chashnikova, M.; Klinkmüller, M.; Fedosenko, O.; MacHulik, S.; Aleksandrova, A.; Monastyrskyi, G.; Flores, Y.; Masselink, W. T. Mid-infrared optical properties of thin films of aluminum oxide, titanium dioxide, silicon dioxide, aluminum nitride, and silicon nitride. *Appl. Opt.* **2012**, *51*, 6789−6798.
(57) Davami, K.; Zhao, L.; Lu, E.; Cortes, J.; Lin, C.; Lilley, D. E.; Purohit, P. K.; Bargatin, I. Ultralight shape-recovering plate mechanical metamaterials. *Nat. Commun.* **2015**, *6*, 1−7.
(58) Holdman, G. R.; Jaffe, G. R.; Jang, M. S.; Feng, D.; Kats, M. A.; Brar, V. W. Thermal runaway of silicon-based laser sails. *ArXiV* preprint; https://arxiv.org/abs/2110.06185, 2021.
(59) Cui, S.; Hu, B.; Ouyang, B.; Zhao, D. Thermodynamic assessment of the Mo-S system and its application in thermal decomposition of MoS_2. *Thermochim. Acta* **2018**, *660*, 44−55.
(60) Cannon, P. Melting point and sublimation of molybdenum disulphide. *Nature* **1959**, *183*, 1612−1613.
(61) Liu, H. L.; Yang, T.; Chen, J. H.; Chen, H. W.; Guo, H.; Saito, R.; Li, M. Y.; Li, L. J. Temperature-dependent optical constants of monolayer MoS_2, $MoSe_2$, WS_2, and WSe_2: spectroscopic ellipsometry and first-principles calculations. *Sci. Rep.* **2020**, *10*, 1−11.
(62) Boccara, A. C.; Jackson, W.; Amer, N. M.; Fournier, D. Sensitive photothermal deflection technique for measuring absorption in optically thin media. *Opt. Lett.* **1981**, *6*, 51.
(63) Keevers, M. J.; Green, M. A. Absorption edge of silicon from solar cell spectral response measurements. *Appl. Phys. Lett.* **1995**, *66*, 174−176.
(64) Edelberg, D.; et al. Approaching the intrinsic limit in transition metal diselenides via point defect control. *Nano Lett.* **2019**, *19*, 4371−4379.
(65) Patil, V.; Kim, J.; Agrawal, K.; Park, T.; Yi, J.; Aoki, N.; Watanabe, K.; Taniguchi, T.; Kim, G.-H. High mobility field-effect transistors based on MoS_2 crystals grown by the flux method. *Nanotechnology* **2021**, *32*, 325603.
(66) Zhang, X.; Lou, F.; Li, C.; Zhang, X.; Jia, N.; Yu, T.; He, J.; Zhang, B.; Xia, H.; Wang, S.; Tao, X. Flux method growth of bulk MoS_2 single crystals and their application as a saturable absorber. *CrystEngComm* **2015**, *17*, 4026−4032.
(67) Yu, Z.; Raman, A.; Fan, S. Fundamental limit of nanophotonic light trapping in solar cells. *Proc. Natl. Acad. Sci. U.S.A.* **2010**, *107*, 17491−17496.
(68) Yu, Z.; Raman, A.; Fan, S. Thermodynamic upper bound on broadband light coupling with photonic structures. *Phys. Rev. Lett.* **2012**, *109*, 1−5.

https://doi.org/10.1021/acs.nanolett.1c03273
Nano Lett. 2022, 22, 594−601